ACS APPLIED MATERIALS & INTERFACES

Research Article

Cite This: ACS Appl. Mater. Interfaces 2019, 11, 42528−42533

www.acsami.org

Proximity Engineering of the van der Waals Interaction in Multilayered Graphene

Sera Kim,[†,‡,∥] Jongho Park,[†,‡,∥] Dinh Loc Duong,[†,‡] Suyeon Cho,[§] Sung Wng Kim,*[,†] and Heejun Yang*[,†]

[†]Department of Energy Science, Sungkyunkwan University, Suwon 16419, Gyeonggi-do, Korea

[‡]Center for Integrated Nanostructure Physics, Institute for Basic Science (IBS), Suwon 16419, Gyeonggi-do, Korea

[§]Division of Chemical Engineering and Materials Science, Ewha Womans University, Seoul 03760, Korea

Supporting Information

ABSTRACT: The van der Waals (vdW) interaction in two-dimensional (2D)-layered materials affects key characteristics of electronic devices, such as the contact resistance, with a vertical heterostructure geometry. While various functionalizations to manipulate the properties of 2D materials have shown issues such as defect generation or have a limited spatial range for the methods, engineering the vdW interaction in nondestructive ways for device applications has not been tried or properly achieved yet. Here, we introduce the proximity engineering of the vdW interaction in multilayered graphene, which is observed as modified interlayer distances and deviated stacking orders by Raman spectroscopy. A 2D electride, $[Ca_2N]^+ \cdot e^-$, possessing a low-work function of 2.6 eV, was used to trigger an avalanche of electrons over tens of graphene layers, exceeding the conventional spatial-range limit (∼1 nm) by screening with a carrier density of 10^{14} cm^{-2}. Our proximity engineering reduces the vdW interaction in a nondestructive way and achieves a promising graphene−metal contact resistance of 500 Ω·μm without using complicated edge contacts, which demonstrates a way to use moderately decoupled graphene layers for device applications.

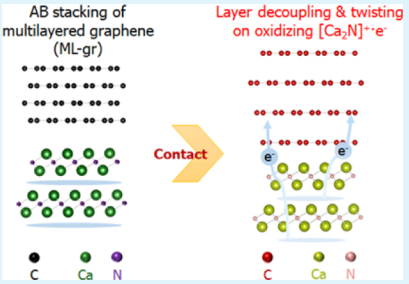

KEYWORDS: *proximity engineering, van der Waals interaction, multilayered graphene, contact resistance, electride*

1. INTRODUCTION

van der Waals (vdW) interaction is a key parameter to determine the electronic properties of graphene and other layered materials, which has opened the door for original nano and quantum electronic devices with two-dimensional (2D)-layered materials.[1−8] In particular, the linear band dispersion of monolayer graphene, a key feature of decoupled graphene, is modified to quadratic energy dispersion in multilayered graphene because of the vdW interaction between layers. The vdW interaction has motivated the investigation of the monolayer and multilayered graphene in terms of band gap opening with symmetry breaking,[4] flat band formation for superconductivity,[5] and carrier doping.[6]

Carrier doping and other functionalizations of graphene for device and catalysis applications have been explored by various methods including nitrogen atom substitution,[9] molecular adsorption,[6] intercalation, and plasma treatment.[10,11] Despite improved performances by these functionalizations, the intrinsic limits of the methods have also been revealed. For example, the effective range of the physical or chemical processes is limited to less than 1 nm by the functionalizations, which originates from a fundamental physical origin, the Thomas−Fermi screening.[12] Moreover, the violent processes for functionalization inevitably induce physical and chemical defects that fatally degrade the high carrier mobility of graphene in device applications, which can be observed by both electrical (measuring field-effect mobility) and optical (Raman spectroscopy) studies.[13] We note that original nanoscopic probe techniques have been developed to properly investigate the characteristics of graphene with low contact resistances.[14−16]

A novel approach for nondestructive and long-range doping of a 2D material, $MoTe_2$, with a 2D electride of $[Ca_2N]^+ \cdot e^-$ has been reported.[12,17,18] The previous study, supported by first-principles calculations, showed that there is an avalanche of electrons from the 2D electride to $MoTe_2$ over a distance of 100 nm through the layer direction, producing a high doping density of 10^{14} cm^{-2} in a large space of the material. In the case of $MoTe_2$, the high carrier density induces a structural phase transition from a hexagonal (semiconducting) to a monoclinic (metallic) structure, exceeding the distance limited by conventional screening.[12,19] We note that the high doping density (10^{14} cm^{-2}) is also available by ionic gating, but the effective range is still limited to 1 nm, which cannot be used for high carrier doping of practical, multilayered 2D materials.

Here, we report a unique manipulation of the vdW interaction in multilayered graphene (over tens of layers) via an exceptionally high-density charge transfer by contacting the

Received: September 14, 2019
Accepted: October 28, 2019
Published: October 28, 2019

DOI: 10.1021/acsami.9b16655
ACS Appl. Mater. Interfaces 2019, 11, 42528−42533

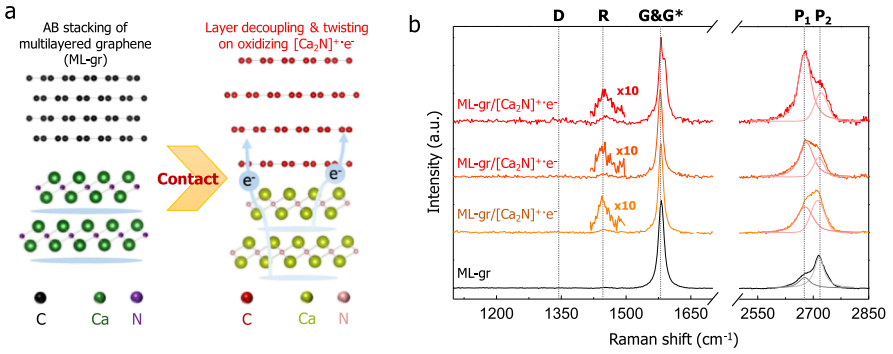

Figure 1. Contact-driven charge transfer to multilayered graphene (ML-gr) on oxidizing $[Ca_2N]^+ \cdot e^-$. (a) Schematic picture of the charge transfer to the ML-gr. Electron layers in the $[Ca_2N]^+ \cdot e^-$ are indicated as blue ellipses, which are weakened after the contact because of the spontaneous electron transfer (oxidation). Carbon lattices after the contact are described as red circles to indicate the resulting interlayer-decoupling and strengthened 2D nature in the ML-gr. (b) Raman spectra of the ML-gr/$[Ca_2N]^+ \cdot e^-$ (top three curves) and a reference ML-gr/SiO_2 (bottom black curve). The mild red and orange colors in the second and third curves (from the top) indicate that the doping concentration is lower than the first curve possibly because of the local geometry of the underlying $[Ca_2N]^+ \cdot e^-$. Clear enhancement of the R peak without generating a D peak reveals the twisting feature of the ML-gr. The increase of the P1 peak component shows the decoupling of the individual layers in the ML-gr/$[Ca_2N]^+ \cdot e^-$.

multilayered graphene with $[Ca_2N]^+ \cdot e^-$. The Raman spectra of the multilayered graphene on $[Ca_2N]^+ \cdot e^-$ show three modified peaks: G, R, and 2D peaks. We did not observe the D peak in all our measurements, indicating that there is no unexpected intercalation of calcium atoms or other impurities into the graphene to create defects, which highlights our method as a nondestructive engineering. While the G peak exhibits a shift originating from the electron doping, the newly-appeared R peak implies that each graphene layer in the multilayered graphene is slightly twisted and deviated from the conventional AB stacking of the graphite. Besides the stacking deviation, the reduced vdW interaction or moderately decoupling graphene layers is demonstrated by the modified 2D peak. Finally, the proximity engineering of the vdW interaction achieves a low practical contact resistance of 500 $\Omega \cdot \mu$m without fabricating a complicated edge contact to the metal electrodes, which opens the way for device applications with moderately decoupled graphene layers.

2. EXPERIMENTAL SECTION

2.1. Fabrication of a Heterostructure, Graphene on $[Ca_2N]^+ \cdot e^-$. The $[Ca_2N]^+ \cdot e^-$, a 2D electride, is a strong reducing agent with an extremely low-work function down to 2.6 eV.[20] The 2D electride possesses delocalized electron layers, described as blue layers in Figure 1a, enabling spontaneous and efficient charge transfer into adjacent materials. The contact-induced avalanche of electrons from the 2D electride is schematically shown in Figure 1a (right side). During the charge transfer, the interlayer distance of the graphene layer changes; the AB stacking of the graphene, represented as the black circles before the contact (left, Figure 1a), is modified to the red circles after the contact (right, Figure 1a). Because of the charge transfer into graphene, the underneath $[Ca_2N]^+ \cdot e^-$ is oxidized, which is described by different colors for the calcium and nitrogen atoms and by the reduced electron layers in Figure 1a. While the contact was made in a glovebox described in the Supporting Information, the $[Ca_2N]^+ \cdot e^-$ oxidized by the subtraction of the electrons, shown in Figure 1a, makes the Raman spectrum similar to that observed with the $[Ca_2N]^+ \cdot e^-$ oxidized in air.[12]

3. RESULTS AND DISCUSSION

It has been reported that the 2D peak in Raman spectroscopy reflects the vdW interaction in multilayered graphene.[21−24] Accordingly, the Raman spectra at three locations, showing a reduced vdW interaction to three different degrees in the multilayered graphene, are shown in Figure 1b (three curves from the top) with a reference Raman spectrum from a flake of AB-stacked graphene layers (bottom black curve). The different degrees of the vdW interaction originate from the nonuniform local charge densities; the local geometry of $[Ca_2N]^+ \cdot e^-$, such as atomic steps with different facets, gives locally different electron-doping densities to the adjacent multilayered graphene. The G and 2D peaks in Figure 1b are carefully fitted by the prominent modes in graphene, and the results are summarized in Figures 1b, S1, and Table S1. We note that there is no D peak around 1350 cm^{-1} in Figure 1b, indicating that the proximity engineering in Figure 1a is nondestructive.

The large amount of electron transfer from $[Ca_2N]^+ \cdot e^-$ to the multilayered graphene achieves a decoupling of the individual graphene layers with a twist between the layers. In particular, the peak component assigned to P1 (2677 cm^{-1}) in Figure 1b represents the 2D nature of the multilayered graphene, which can be considered as a stacking of decoupled graphene monolayers. In contrast, the peak component assigned to P2 (2715 cm^{-1}) in Figure 1b indicates a three-dimensional nature, originating from the interacting graphene layers mostly with an AB stacking order (i.e., conventional vdW interaction in the graphite). The Raman spectra in Figure 1b show an increase of the P1 component with respect to the P2 component; the P1 to P2 ratio changes from 0.34 (derived from the black curve from the conventional graphite) to 2.38 (derived from the top red curve from the multilayered graphene on $[Ca_2N]^+ \cdot e^-$).

There are two emerging peak components in the Raman spectra of the multilayered graphene on $[Ca_2N]^+ \cdot e^-$ in Figure 1b. The R peak located at around 1451 cm^{-1}, which has been known as a sign of twisted graphene layers, is newly observed in the red curves (top three curves) in Figure 1b. The other peak component, which is mostly called the G* peak around 1588 cm^{-1}, is also observed in the multilayered graphene; the G* peak has been known to be evidence of disorders in graphene. The Raman features in Figure 1b imply that the electron avalanche into the multilayered graphene via physical contact to $[Ca_2N]^+ \cdot e^-$ results in decoupling (an increase of the P1 peak) and twisting (emerging R peak) of the individual graphene layers with a certain domain or grain nature (G* peak); we speculate that the disorder feature (G* peak)

DOI: 10.1021/acsami.9b16655
ACS Appl. Mater. Interfaces 2019, 11, 42528−42533

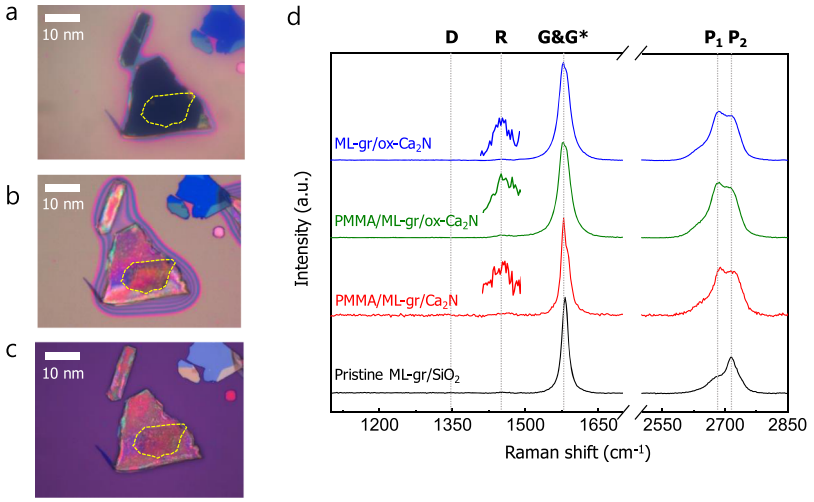

Figure 2. Stability of the electron-doped ML-gr/$[Ca_2N]^+\cdot e^-$. (a–c) The optical images of the PMMA/ML-gr/$[Ca_2N]^+\cdot e^-$ in an Ar-filled glovebox, PMMA/ML-gr/oxidized $[Ca_2N]^+\cdot e^-$ in air, and ML-gr/oxidized $[Ca_2N]^+\cdot e^-$ after the removal of the top PMMA film in air, respectively. (d) Raman spectra of the sample in (a) (red curve), (b) (green curve), and (c) (blue curve) with a reference ML-graphene/SiO_2 (black curve).

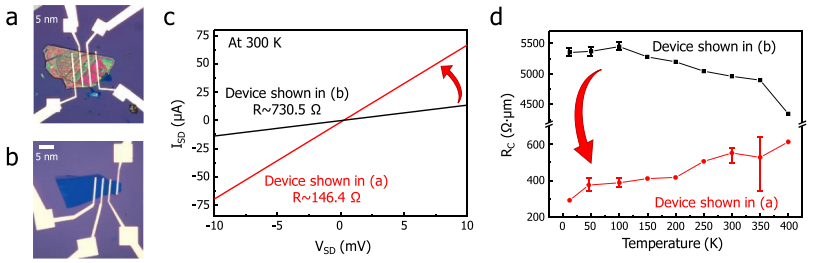

Figure 3. Device characteristics of the ML-gr/$[Ca_2N]^+\cdot e^-$ and ML-gr/SiO_2. (a,b) The optical images of a four-terminal device with the ML-gr//$[Ca_2N]^+\cdot e^-$ and ML-gr/SiO_2, respectively. (c) Source–drain two-terminal current (I_{SD}) measurements as a function of the voltage (V_{SD}) with the device in (a) (red curve) and (b) (black curve). (d) Contact resistance (R_C) was derived by four-terminal measurements with the device in (a,b). Then, the R_C values at various temperatures are plotted for the devices in (a,b).

originates from the locally different degrees of doping concentrations by the locally varying work function of $[Ca_2N]^+\cdot e^-$.[12]

The stability of the highly electron-doped graphene on $[Ca_2N]^+\cdot e^-$ against air exposure and postoxidation of the substrate was investigated and is summarized in Figure 2. The fabrication of the multilayered graphene on $[Ca_2N]^+\cdot e^-$ was done with a passivation layer [poly(methyl methacrylate), PMMA] in our glovebox, and a photograph of the stacked sample is shown in Figure 2a; the surfaces of the $[Ca_2N]^+\cdot e^-$ and graphene are maintained intact and flat without any oxidation in the glovebox. Although the $[Ca_2N]^+\cdot e^-$ flake was covered by a multilayered graphene flake and additional PMMA passivation layer, the underlying $[Ca_2N]^+\cdot e^-$ flake can be easily oxidized outside the glovebox,[9] as shown in Figure 2b. A fully oxidized $[Ca_2N]^+\cdot e^-$ flake after air exposure shows a clear optical contrast by its increased surface roughness, as shown in Figure 2b.

The Raman features for the reduced vdW interaction in multilayered graphene were maintained by air exposure (postoxidation), as shown in Figure 2b. Moreover, the adhesion of the highly electron-doped graphene to oxidized $[Ca_2N]^+\cdot e^-$ is stable enough to be kept in chemical treatments such as removing the PMMA by acetone rinsing. An optical image of the multilayered graphene on $[Ca_2N]^+\cdot e^-$ after removing the passivation layer (PMMA) in air is shown in Figure 2c. As summarized in Figure 2d, the major features, modified ratio of P1 to P2 and the emerging R and G* peaks, are identically observed in the multilayered graphene on the postoxidized $[Ca_2N]^+\cdot e^-$ before and after the removal of the PMMA (green and blue curves in Figure 2d). We note that the stability against air exposure and various chemical treatments is critical for device applications.

To exclude other possible origins such as strain effect from the bottom substrate for the unique Raman features in Figures 1 and 2, we conducted a comparison measurement with the multilayered graphene on pre-oxidized $[Ca_2N]^+\cdot e^-$. In the comparison experiment, the $[Ca_2N]^+\cdot e^-$ flakes were intentionally oxidized first, and then, multilayered graphene flakes were transferred onto the pre-oxidized $[Ca_2N]^+\cdot e^-$, as shown in Figure S2; the thickness and relative geometry between the two flakes in Figure S2 were chosen to be same as those in Figure 2. The Raman spectra in Figure S2 do not show meaningful changes, indicating that the unique Raman characteristics in Figure 2 do not originate from other geometrical reasons, such as strain, with the flakes having rough surfaces. Thus, the large amount of electron transfer from the pristine $[Ca_2N]^+\cdot e^-$ to graphene is considered as the key origin for the Raman spectra in Figures 1 and 2.

As the electron transfer occurs at the interface between the multilayered graphene and $[Ca_2N]^+\cdot e^-$, which is located at the bottom of the multilayered graphene, it is critical to investigate how far the electron doping can reach through the vdW gaps between the graphene layers. We note that the Raman

DOI: 10.1021/acsami.9b16655
ACS Appl. Mater. Interfaces 2019, 11, 42528–42533

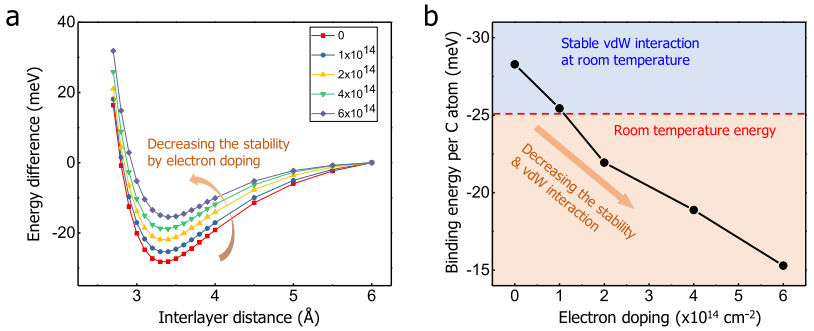

Figure 4. First-principles calculations for the interlayer interaction in the ML-gr as a function of the interlayer distance and doping concentration. (a) Stability change by the doping concentration and interlayer distance. (b) Interlayer binding energy, extracted from the minimum energy in (a) for each doping concentration.

measurements in Figures 1 and 2 do not have the spatial resolution in the vertical direction. The thickness of the multilayered graphene in our study was around 5 nm (~15 layers of graphene). The screening length or Debye length (L_D) is given by the formula $L_D \equiv \sqrt{\frac{\epsilon kT}{q^2 N}}$, where ε, k, and N are the dielectric constant, Boltzmann constant, and carrier density, respectively; the value of L_D becomes 1 nm at a carrier density (N) of 10^{14} cm^{-2} or 10^{21} cm^{-3}, which is much shorter than the thickness of the multilayered graphene in our study (5 nm). Nevertheless, we could observe a modification of the top graphene layer by proximity engineering at the bottom of the multilayered graphene, which is useful for device applications.

The top graphene layer, influenced by the doping from the bottom graphene layer, could be studied by measuring the contact resistance between the top graphene layer and another metal electrode following a conventional metallization process, which is also an important subject for device applications. It has been known that the contact resistance changes by the doping level of the top graphene layer. Four-probe electronic devices were fabricated to measure the contact resistances in the two systems shown in Figure 3. Multilayered graphene flakes with the same thickness on $[Ca_2N]^+\cdot e^-$ (Figure 3a) and on SiO_2 (Figure 3b) were investigated. The $[Ca_2N]^+\cdot e^-$ was oxidized during the device fabrication, but the doping of the multilayered graphene could be maintained as we discussed with Figure 2. To compare the two contact resistances, the same metals, chrome (Cr) and gold (Au), were used for the electrodes.

The overall two-probe resistance was decreased by more than five times in the 5 nm thick multilayered graphene on $[Ca_2N]^+\cdot e^-$ shown in Figure 3c. Because of the absence of the band gap in graphene, the conductance modulation of the multilayered graphene up to five times is exceptional, which has not been achieved by conventional electric gating[25] or molecular doping.[13] We note that the screening theory in physics restricts such a large conductivity modulation over the thickness (~5 nm) of semimetals (e.g., graphite) by the doping or gating method, which demonstrates the unique function of our proximity engineering based on the avalanche of electrons from the 2D electride.

Because the channel resistance and contact resistance are equally involved in the two-probe measurement, the contact resistance, R_C, was separately studied by the four-probe measurement shown in Figure 3d. The R_C decreases to 500 $\Omega\cdot\mu$m with the underlying $[Ca_2N]^+\cdot e^-$ (red points in Figure 3d), which is nine times lower that of the pristine multilayered graphene (black points in Figure 3d). The R_C decreases even further at lower temperatures shown in Figure 3d. The reduced R_C is similar to that from the graphene edge contact; we achieved this promising contact for device applications without using complicated fabrication methods for the edge contact.[26] The transport data are easily reproducible with the 5 nm thick multilayered graphene on pristine $[Ca_2N]^+\cdot e^-$; pre-oxidized $[Ca_2N]^+\cdot e^-$ cannot produce the reduced R_C.

Concerning the channel resistance, semiconducting behavior (increasing resistance at a lower temperature) of the channel was observed as shown in Figure S3 (red curve). The pristine multilayered graphene shows a constant resistance at varying temperatures (black curve in Figure S3), which can be understood by the semimetallic characteristics of the pristine multilayered graphene. We explain that the semiconducting behavior in Figure S3 (red curve) originates from numerous carrier scatterings in the multilayered graphene with the reduced vdW interaction on the rough substrate of the postoxidized $[Ca_2N]^+\cdot e^-$. Despite the increased scattering in lateral transport, most vertical transport properties for practical device applications with a vdW heterostructure geometry mainly require contact resistance, which is not influenced by the oxidation of $[Ca_2N]^+\cdot e^-$.

To understand the decoupling and twisting features in the heavily doped multilayered graphene, we conducted first-principles calculations on the interlayer interaction and distances with different doping concentrations and interlayer distances. The interlayer distance could be found by the minimum energy, as shown in Figure 4a, and the value shows that the interlayer distance of graphene is almost unchanged by increasing the electron density up to 6×10^{14} cm^{-2}. However, the interlayer interaction, which is required to get isolated graphene layers, becomes weaker, which indicates a possible decoupling of individual graphene layers. Figure 4b shows the decreasing interlayer binding energy between the carbon atoms in the adjacent layers for the increasing electron-doping concentration. Therefore, the first-principles calculations support our experimental findings of interlayer decoupling in the multilayered graphene via heavy electron doping from the $[Ca_2N]^+\cdot e^-$ electride (proximity engineering).

4. CONCLUSIONS

A novel and nondestructive way of electron doping up to 10^{14} cm^{-2} over a long vertical distance in multilayered graphene (up to 5 nm) was developed by proximity engineering with a 2D electride, $[Ca_2N]^+\cdot e^-$. Raman spectra and transport studies

DOI: 10.1021/acsami.9b16655
ACS Appl. Mater. Interfaces 2019, 11, 42528−42533

demonstrate that the individual graphene layers are moderately decoupled and twisted by the avalanche of electrons in the multilayered graphene, which is supported by first-principles calculations. The proximity engineering improves the top contact resistance for the first time, making it nine times lower than that of pristine multilayered graphene without using complicated fabrication methods for the edge contact. These findings pave the way to use moderately decoupled graphene layers for device applications.

■ ASSOCIATED CONTENT

Supporting Information

The Supporting Information is available free of charge on the ACS Publications website at DOI: 10.1021/acsami.9b16655.

Sample preparation, fitted G mode in the Raman spectra of the graphite and decoupled graphite, Raman spectra of the ML grapheme, temperature-dependent 4-terminal resistance of the ML graphene, and fitting parameters of the Raman spectra (PDF)

■ AUTHOR INFORMATION

Corresponding Authors

*E-mail: kimsungwng@skku.edu (S.W.K.).
*E-mail: h.yang@skku.edu (H.Y.).

ORCID

Dinh Loc Duong: 0000-0002-4118-9589
Suyeon Cho: 0000-0003-1931-9663
Sung Wng Kim: 0000-0002-4802-5421
Heejun Yang: 0000-0003-0502-0054

Author Contributions

‖S.K. and J.P. contributed equally to this work.

Notes

The authors declare no competing financial interest.

■ ACKNOWLEDGMENTS

This work is supported by the National Research Foundation of Korea (NRF) under grant no. NRF-2017R1A2B2008366. S.C. was supported by the Basic Science Research Program through the National Research Foundation of Korea (NRF) funded by the Ministry of Science, ICT and Future Planning (2017R1A2B4010423). D.L.D. was supported by the Institute for Basic Science (IBS-R011-D1), Korea. J.P. and S.W.K. were supported by a National Research Foundation of Korea (NRF) grant funded by the Korean government (Ministry of Science, ICT & Future Planning) (No. 2015M3D1A1070639).

■ REFERENCES

(1) Zhang, Y.; Tan, Y.-W.; Stormer, H. L.; Kim, P. Experimental Observation of the Quantum Hall Effect and Berry's Phase in Graphene. *Nature* **2005**, *438*, 201−204.

(2) Novoselov, K. S.; McCann, E.; Morozov, S. V.; Fal'ko, V. I.; Katsnelson, M. I.; Zeitler, U.; Jiang, D.; Schedin, F.; Geim, A. K. Unconventional Quantum Hall effect and Berry's Phase of 2π in Bilayer Graphene. *Nat. Phys.* **2006**, *2*, 177−180.

(3) Yang, H.; Heo, J.; Park, S.; Song, H. J.; Seo, D. H.; Byun, K.-E.; Kim, P.; Yoo, I.; Chung, H.-J.; Kim, K. Graphene Barristor, a Triode Device with a Gate-Controlled Schottky Barrier. *Science* **2012**, *336*, 1140−1143.

(4) Zhang, Y.; Tang, T.-T.; Girit, C.; Hao, Z.; Martin, M. C.; Zettl, A.; Crommie, M. F.; Shen, Y. R.; Wang, F. Direct Observation of a Widely Tunable Bandgap in Bilayer Graphene. *Nature* **2009**, *459*, 820−823.

(5) Cao, Y.; Fatemi, V.; Fang, S.; Watanabe, K.; Taniguchi, T.; Kaxiras, E.; Jarillo-Herrero, P. Unconventional Superconductivity in Magic-Angle Graphene Superlattices. *Nature* **2018**, *556*, 43−50.

(6) Zhang, W.; Lin, C.-T.; Liu, K.-K.; Tite, T.; Su, C.-Y.; Chang, C.-H.; Lee, Y.-H.; Chu, C.-W.; Wei, K.-H.; Kuo, J.-L.; Li, L.-J. Opening an Electrical Band Gap of Bilayer Graphene with Molecular Doping. *ACS Nano* **2011**, *5*, 7517.

(7) Keum, D. H.; Cho, S.; Kim, J. H.; Choe, D.-H.; Sung, H.-J.; Kan, M.; Kang, H.; Hwang, J.-Y.; Kim, S. W.; Yang, H.; Chang, K. J.; Lee, Y. H. Bandgap Opening in Few-Layered Monoclinic $MoTe_2$. *Nat. Phys.* **2015**, *11*, 482−486.

(8) Cho, S.; Kim, S.; Kim, J. H.; Zhao, J.; Seok, J.; Keum, D. H.; Baik, J.; Choe, D.-H.; Chang, K. J.; Suenaga, K.; Kim, S. W.; Lee, Y. H.; Yang, H. Phase Patterning for Ohmic Homojunction Contact in $MoTe_2$. *Science* **2015**, *349*, 625−628.

(9) Panchakarla, L. S.; Subrahmanyam, K. S.; Saha, S. K.; Govindaraj, A.; Krishnamurthy, H. R.; Waghmare, U. V.; Rao, C. N. R. Synthesis, Structure, and Properties of Boron- and Nitrogen-Doped Graphene. *Adv. Mater.* **2009**, *21*, 4726−4730.

(10) Profeta, G.; Calandra, M.; Mauri, F. Phonon-Mediated Superconductivity in Graphene by Lithium Deposition. *Nat. Phys.* **2012**, *8*, 131−134.

(11) Eshete, Y. A.; Ling, N.; Kim, S.; Kim, D.; Hwang, G.; Cho, S.; Yang, H. Vertical Heterophase for Electrical, Electrochemical, and Mechanical Manipulations of Layered $MoTe_2$. *Adv. Funct. Mater.* **2019**, *29*, 1904504.

(12) Kim, S.; Song, S.; Park, J.; Yu, H. S.; Cho, S.; Kim, D.; Baik, J.; Choe, D.-H.; Chang, K. J.; Lee, Y. H.; Kim, S. W.; Yang, H. Long-Range Lattice Engineering of $MoTe_2$ by a 2D Electride. *Nano Lett.* **2017**, *17*, 3363−3368.

(13) Kurapati, R.; Mukherjee, S. P.; Martín, C.; Bepete, G.; Vázquez, E.; Pénicaud, A.; Fadeel, B.; Bianco, A. Degradation of Single-Layer and Few-Layer Graphene by Neutrophil Myeloperoxidase. *Angew. Chem., Int. Ed.* **2018**, *57*, 11722−11727.

(14) Bøggild, P.; Mackenzie, D. M. A.; Whelan, P. R.; Petersen, D. H.; Buron, J. D.; Zurutuza, A.; Gallop, J.; Hao, L.; Jepsen, P. U. Mapping the Electrical Properties of Large-area Graphene. *2D Mater* **2017**, *4*, 042003.

(15) Aprojanz, J.; Power, S. R.; Bampoulis, P.; Roche, S.; Jauho, A.-P.; Zandvliet, H.; Zakharov, A. A.; Tegenkamp, C. Ballistic Tracks in Graphene Nanoribbons. *Nat. Commun.* **2018**, *9*, 4426.

(16) Zhao, M.; Kim, D.; Nguyen, V. L.; Jiang, J.; Sun, L.; Lee, Y. H.; Yang, H. Coherent Thermoelectric Power from Graphene Quantum Dots. *Nano Lett.* **2019**, *19*, 61−68.

(17) Tang, Q. Enhanced 1T′-Phase Stabilization and Chemical Reactivity in a $MoTe_2$ Monolayer through Contact with a 2D Ca_2N Electride. *ChemPhysChem* **2019**, *20*, 595−601.

(18) Inoshita, T.; Tsukada, M.; Saito, S.; Hosono, H. Probing a Divergent van Hove Singularity of Graphene With a Support: A Layered Electride as a Solid-State Dopant. *Phys. Rev. B* **2017**, *96*, 245303−245310.

(19) Seok, J.; Lee, J.-H.; Cho, S.; Ji, B.; Kim, H. W.; Kwon, M.; Kim, D.; Kim, Y.-M.; Oh, S. H.; Kim, S. W.; Lee, Y. H.; Son, Y.-W.; Yang, H. Active Hydrogen Evolution through Lattice Distortion in Metallic $MoTe_2$. *2D Mater.* **2017**, *4*, 025061−025068.

(20) Lee, K.; Kim, S. W.; Toda, Y.; Matsuishi, S.; Hosono, H. Dicalcium Nitride as a Two-Dimensional Electride with an Anionic Electron Layer. *Nature* **2013**, *494*, 336−340.

(21) Wu, J.-B.; Hu, Z.-X.; Zhang, X.; Han, W.-P.; Lu, Y.; Shi, W.; Qiao, X.-F.; Ijiäs, M.; Milana, S.; Ji, W.; Ferrari, A. C.; Tan, P.-H. Interface Coupling in Twisted Multilayer Graphene by Resonant Raman Spectroscopy of Layer Breathing Modes. *ACS Nano* **2015**, *9*, 7440−7449.

(22) Niilisk, A.; Kozlova, J.; Alles, H.; Aarik, J.; Sammelselg, V. Raman Characterization of Stacking in Multi-layer Graphene Grown on Ni. *Carbon* **2016**, *98*, 658−665.

(23) Wu, J.-B.; Lin, M.-L.; Cong, X.; Liu, H.-N.; Tan, P.-H. Raman Spectroscopy of Graphene-Based Materials and Its Applications in Related Devices. *Chem. Soc. Rev.* **2018**, *47*, 1822−1873.

DOI: 10.1021/acsami.9b16655
ACS Appl. Mater. Interfaces 2019, 11, 42528−42533

(24) Yang, H.; Kim, S. W.; Chhowalla, M.; Lee, Y. H. Structural and Quantum-State Phase Transition in Van der Waals Layered Materials. *Nat. Phys.* **2017**, *13*, 931−937.
(25) Sui, Y.; Appenzeller, J. Multi-Layer Graphene Field-Effect Transistors for Improved Device Performance. *2009 Device Research Conference*, 2009.
(26) Wang, L.; Meric, I.; Huang, P. Y.; Gao, Q.; Gao, Y.; Tran, H.; Taniguchi, T.; Watanabe, K.; Campos, L. M.; Muller, D. A.; Guo, J.; Kim, P.; Hone, J.; Shepard, K. L.; Dean, C. R. One-Dimensional Electrical Contact to a Two-Dimensional Material. *Science* **2013**, *342*, 614−617.

DOI: 10.1021/acsami.9b16655
ACS Appl. Mater. Interfaces 2019, 11, 42528−42533